A comparative study of CCl_4 reactions on Ag and Si surfaces by *in situ* ultraviolet photoemission electron microscopy

2009 J. Phys.: Condens. Matter 21 314014

(http://iopscience.iop.org/0953-8984/21/31/314014)

J. Phys.: Condens. Matter **21** (2009) 314014 (7pp) doi:10.1088/0953-8984/21/31/314014

A comparative study of CCl_4 reactions on Ag and Si surfaces by *in situ* ultraviolet photoemission electron microscopy

Yunxi Yao, Qiang Fu, Dali Tan and Xinhe Bao

State Key Laboratory of Catalysis, Dalian Institute of Chemical Physics,
The Chinese Academy of Sciences, Dalian 116023, People's Republic of China

E-mail: qfu@dicp.ac.cn and xhbao@dicp.ac.cn

Received 31 December 2008, in final form 10 April 2009
Published 7 July 2009
Online at stacks.iop.org/JPhysCM/21/314014

Abstract

The reactivity of a bulk Ag surface, an Ag monolayer film on Si(111)-7 × 7 (denoted as the $\sqrt{3} \times \sqrt{3}$-Ag–Si surface), and Si(111)-7 × 7 to CCl_4 was investigated by x-ray photoelectron spectroscopy (XPS) and ultraviolet photoemission electron microscopy (UV-PEEM). *In situ* UV-PEEM was used to monitor simultaneously the CCl_4 dissociation on different surface domains, including the bulk Ag, $\sqrt{3} \times \sqrt{3}$-Ag–Si, and Si(111). The PEEM results combined with XPS data show that CCl_4 adsorbs dissociatively on bulk Ag(111) and Si(111) but adsorbs molecularly on the $\sqrt{3} \times \sqrt{3}$-Ag–Si surface, and the surface reactivity follows the order of Si(111) > Ag(111) > $\sqrt{3} \times \sqrt{3}$-Ag–Si.

(Some figures in this article are in colour only in the electronic version)

1. Introduction

Dynamics at catalyst surfaces is among the most important issues in heterogeneous catalysis [1]. Photoemission electron microscopy (PEEM) is a dedicated surface imaging technique with spatial resolution at the nanoscale (e.g. <20 nm for the aberration corrector-type PEEM) and high temporal resolution of millisecond level (<10 ms), which presents as a powerful tool for investigating the surface dynamic processes, such as surface reactions, surface diffusion, film growth, and surface phase transition. For example, CO and H_2 oxidation on Pt(100) and Pt(110) surfaces has been imaged by PEEM, and nonlinear reaction kinetics was clearly derived on the basis of the *in situ* PEEM data [2–5]. Evolution of pentacene thin films on Si(001) has been studied by utilizing the real time imaging capabilities of PEEM, which enables understanding of the thin film growth process [6, 7]. Moreover, PEEM can be used to image a surface region containing various surface domains, and it is possible to compare the reactions at the different surface phases under exactly the same conditions, bypassing the experimental complications of comparing separate measurements on several surfaces [8, 9].

Ag monolayer film can form on Si(111)-7 × 7 with ($\sqrt{3} \times \sqrt{3}$) symmetry; this is known as a $\sqrt{3} \times \sqrt{3}$-Ag–Si surface [10, 11]. Our previous study showed that the Ag monolayer film presents unique surface reactivity compared to bulk Ag(111) surface due to the confinement of Ag 5sp electrons in the Ag monolayer structure [12]. Furthermore, upon formation of the $\sqrt{3} \times \sqrt{3}$-Ag layer on the Si(111)-7 × 7 surface, dangling bonds at the Si adatoms and restatoms have been completely removed by the deposited Ag adatoms. It is expected that the reactivity of the $\sqrt{3} \times \sqrt{3}$-Ag–Si surface should be different from that of the Si(111)-7 × 7 surface. For example, it has been reported that the Si(111) surface became passivated to O_2 and NH_3 adsorption [13, 14] when covered by a $\sqrt{3} \times \sqrt{3}$-Ag layer. Therefore, the $\sqrt{3} \times \sqrt{3}$-Ag–Si surface may present distinct reactivity in comparison with the bulk Ag and Si surfaces.

In the present work, a comparative study in reactivity of the bulk Ag, bulk Si(111), and $\sqrt{3} \times \sqrt{3}$-Ag–Si surfaces was made using x-ray photoelectron spectroscopy (XPS) and UV-PEEM. Dedicated samples have been prepared, which consist of surface domains of the bulk Ag, $\sqrt{3} \times \sqrt{3}$-Ag–Si, and Si(111) surface phases. The dynamics of CCl_4 dissociation reactions on the different surfaces could be simultaneously investigated by PEEM, revealing unambiguously the difference in surface reactivity.

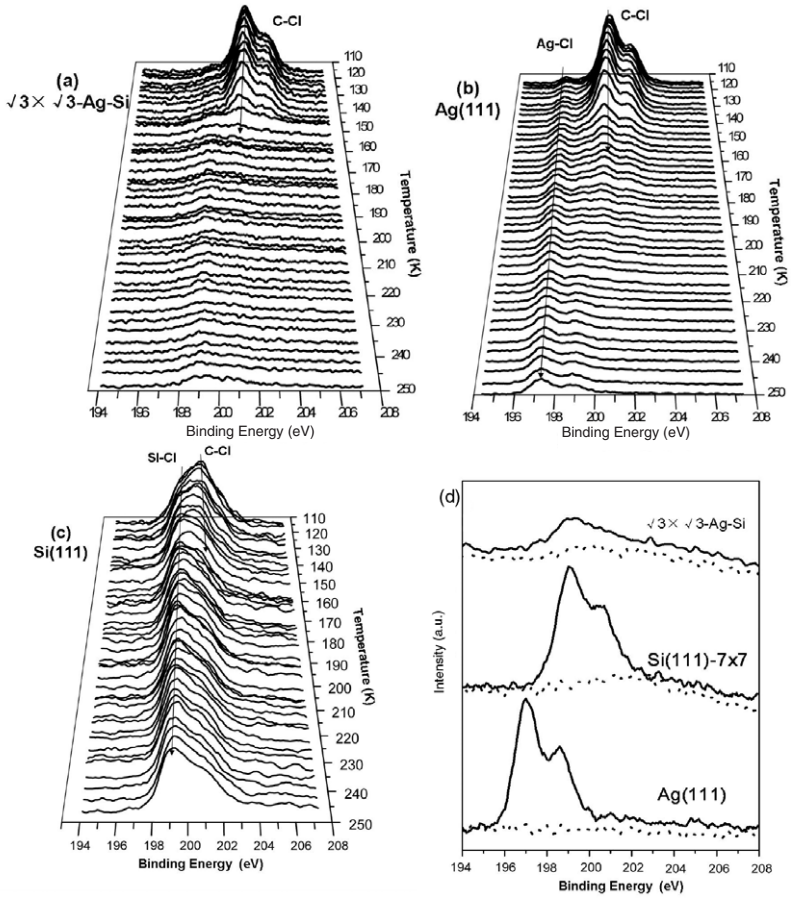

Figure 1. Temperature-programed XPS Cl 2p spectra from (a) the $\sqrt{3} \times \sqrt{3}$-Ag–Si surface, (b) the Ag(111) surface, and (c) the Si(111)-7 × 7 surface, adsorbed with 6 L CCl_4 at about 120 K and subsequently annealed up to 250 K. Each spectrum was acquired in 1 min. Cl 2p signals from molecular CCl_4 (C–Cl) and dissociated atomic Cl species (Ag–Cl and Si–Cl) are labeled in the spectra. (d) XPS Cl 2p spectra from the Ag(111), Si(111), and $\sqrt{3} \times \sqrt{3}$-Ag–Si surfaces before (dotted lines) and after (solid lines) exposure of 9.6, 10.8, and 16.2 L CCl_4 at RT, respectively.

2. Experimental details

All the experiments were performed in an Omicron multiple-chamber ultrahigh vacuum (UHV) system, which was equipped with a hemisphere analyzer (Omicron EA 125 5-channeltron) for XPS, a variable temperature scanning tunneling microscope (STM), and a UV-PEEM (Focus IS-PEEM) [12, 15]. UV-PEEM imaging was conducted at room temperature (RT) using a 100 W mercury short-arc lamp as a radiation source with photon energy of the main UV line at about 4.9 eV. XPS data were collected with Mg Kα (1253.6 eV) radiation. For temperature-programed XPS (TP-XPS) experiments, the sample temperature was ramped up at the rate of 3 K min^{-1} and each spectrum was recorded within 1 min. STM images were recorded in constant current mode using a W tip at RT.

Ag(111) was cleaned by repeated Ar^+ sputtering (1000 eV, 20 μA) and UHV annealing (873 K) until no contaminations were detected. Well ordered Si(111)-7 × 7 surfaces were obtained by direct current heating up to 1473 K several times. Ag was deposited from an effusion cell, which can provide exact control of Ag flux. Ag monolayer film ($\sqrt{3} \times \sqrt{3}$-Ag) was obtained by depositing one monolayer (ML) of Ag on the Si(111)-7 × 7 surface at about 550 K. A sample consisting of surface domains of $\sqrt{3} \times \sqrt{3}$-Ag–Si and bulk Ag phases was prepared by depositing several additional ML of Ag on the $\sqrt{3} \times \sqrt{3}$-Ag–Si surface at 350 K. When a shutter was applied to mask half of the substrate surface, a sample consisting of the $\sqrt{3} \times \sqrt{3}$-Ag–Si, bulk Ag, and Si(111)-7 × 7 surface domains was obtained.

High performance liquid chromatography (HPLC) grade CCl_4 was used and purified by the freeze–pump–thaw technique several times. Sample dosing was performed by backfilling the UHV chamber via a leak valve.

3. Results and discussion

Three surfaces of Ag(111), Si(111)-7 × 7, and $\sqrt{3} \times \sqrt{3}$-Ag–Si have been prepared, and CCl_4 was used as the probe molecule for studying the surface reactivity. CCl_4 adsorption and dissociation on the three surfaces were investigated by TP-XPS. Each surface was exposed to 6 Langmuir (L) CCl_4 at 120 K followed by subsequent annealing up to 250 K with a temperature ramp rate of 3 K min^{-1}. During the annealing process, XPS Cl 2p spectra were recorded and these are shown in figure 1.

On the $\sqrt{3} \times \sqrt{3}$-Ag–Si surface, molecular adsorption of CCl_4 was observed at 120 K, as confirmed by the appearance

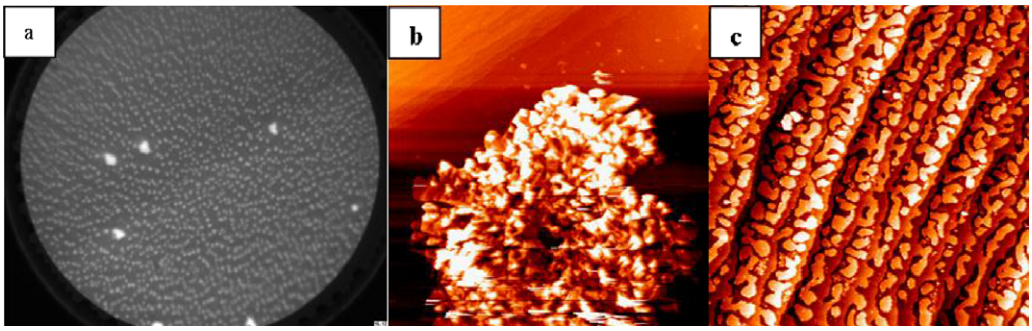

Figure 2. (a) PEEM image (field of view (FoV): 120 μm) of the Ag | $\sqrt{3} \times \sqrt{3}$-Ag–Si surface; (b) STM image (2000 nm × 2000 nm) of the Ag | $\sqrt{3} \times \sqrt{3}$-Ag–Si surface; (c) STM image (500 nm × 500 nm) of the clean $\sqrt{3} \times \sqrt{3}$-Ag–Si region.

of a single Cl 2p $_{3/2}$ peak at 200.7 eV from Cl in the CCl_4 molecule [16] (figure 1(a)). When annealing the surface, the intensity of the Cl 2p spectra decreases quickly, and the complete molecular desorption of CCl_4 happens at ∼160 K. After that, the spectra almost recover the character of a clean $\sqrt{3} \times \sqrt{3}$-Ag–Si surface except that there is a small peak at 199.0 eV from Cl bonded to Si. The residue Cl signals may be produced by CCl_4 dissociation at defect sites of Si, such as steps or missing Ag atoms at the $\sqrt{3} \times \sqrt{3}$-Ag–Si surface. No dissociated Cl species reacted with Ag were observed on the surface.

The Ag(111) surface is reactive to CCl_4 (figure 1(b)). Upon adsorption at 120 K, both molecular adsorption and dissociative adsorption of CCl_4 occur on Ag(111), which was revealed by the appearance of a Cl $2p_{3/2}$ signal centered at 200.5 eV from Cl in CCl_4 and a Cl $2p_{3/2}$ component at 197.4 eV due to atomic Cl species adsorbed on Ag [17]. With increasing annealing temperature, CCl_4 molecules continue to dissociate, which can be seen from the increasing intensity of the Cl species adsorbed on Ag. At the same time, the CCl_4 signal keeps on decreasing and almost disappears from the surface at 180 K.

Compared to both Ag surfaces, the Si(111) is much more reactive to CCl_4. Even at 120 K, a strong Cl 2p signal at 199.0 eV from the dissociated Cl species on Si(111) was detected by XPS. After annealing above 200 K, CCl_4 molecules cannot be observed and only strong Cl species from Cl–Si remain on the surface (figure 1 (c)). The TP-XPS results suggest that the surface reactivity follows the order of Si(111) > Ag(111) > $\sqrt{3} \times \sqrt{3}$-Ag–Si.

In order to confirm the above conclusion further, CCl_4 dissociation at each surface at RT was studied by XPS. As shown in figure 1(d), exposure of 10 L CCl_4 at RT produced strong peaks of dissociated Cl bonded to Ag and Si on the Ag(111) and Si(111) surfaces, respectively. In contrast, only a small peak of Cl from Cl–Si species was found to overlap the broad background on the $\sqrt{3} \times \sqrt{3}$-Ag–Si surface after the CCl_4 adsorption. Therefore, the RT-XPS and TP-XPS results are consistent with each other, indicating the different surface reactivities.

In order to image the reactions at the $\sqrt{3} \times \sqrt{3}$-Ag–Si and bulk Ag surfaces simultaneously by using *in situ* PEEM, a special sample surface was prepared, which consists of surface domains of $\sqrt{3} \times \sqrt{3}$-Ag–Si and bulk Ag. First, 1.6 ML Ag was deposited on the Si(111)-7 × 7 surface at 550 K, and the excess of 1 ML Ag enables the surface to be fully covered by the $\sqrt{3} \times \sqrt{3}$-Ag layer. When the sample was cooled down below 350 K, several additional ML of Ag were evaporated on the as-prepared $\sqrt{3} \times \sqrt{3}$-Ag–Si surface. Due to the low surface free energy of the $\sqrt{3} \times \sqrt{3}$-Ag–Si surface, Ag adatoms are highly diffusive and tend to aggregate to form Ag particles atop [12, 18]. In this way, the coexistence of Ag particles and clean $\sqrt{3} \times \sqrt{3}$-Ag–Si surfaces (denoted as Ag | $\sqrt{3} \times \sqrt{3}$-Ag–Si surfaces) was achieved. A typical PEEM image acquired from the surface is given in figure 2(a), which shows that the surface consists of bright dots with size of 1–2 μm sitting on a dark background. Because of the low density of states (DOS) near the Fermi edge (E_F) at the $\sqrt{3} \times \sqrt{3}$-Ag–Si surface [12], this surface appears darker in the PEEM image in comparison with the bulk Ag surface. Therefore, the bright dots should be attributed to bulk Ag particles and the dark regions are from the bare $\sqrt{3} \times \sqrt{3}$-Ag–Si surface. This surface was also imaged by STM, and the surface morphology is shown in figures 2(b) and (c). Large Ag particles with the size of about 1.8 μm were observed, and the particles consist of many aggregated microcrystallites. Thus, the big Ag particles can be regarded as bulk Ag structure. Between the Ag particles, the $\sqrt{3} \times \sqrt{3}$-Ag–Si surface can be clearly seen, showing the characteristic two-level surface structure [18] (figure 2(c)).

The reactivity of the Ag particles and the $\sqrt{3} \times \sqrt{3}$-Ag–Si surface was studied by using *in situ* PEEM. Figure 3 shows a series of snapshots from the PEEM video acquired from the Ag | $\sqrt{3} \times \sqrt{3}$-Ag–Si surface exposed to different amounts of CCl_4. Before CCl_4 exposure, the bulk Ag particles were brighter than the $\sqrt{3} \times \sqrt{3}$-Ag–Si surface. Upon exposing 5.2×10^{-9} mbar CCl_4 to the surface, the gray intensity at the Ag particles decreases gradually, while there is little change in the brightness at the $\sqrt{3} \times \sqrt{3}$-Ag–Si surface. After about 4000 s the image contrast at the Ag particles and the $\sqrt{3} \times \sqrt{3}$-Ag–Si surface region has been reversed. Figure 3(b) shows the variation of the gray intensity at the Ag particles and $\sqrt{3} \times \sqrt{3}$-Ag–Si surface with the CCl_4 exposure time. We can see that the gray intensity at Ag particles sharply decreases with the CCl_4 exposure time. Eventually, it becomes lower than that at the $\sqrt{3} \times \sqrt{3}$-Ag–Si surface. In contrast, the gray intensity at the $\sqrt{3} \times \sqrt{3}$-Ag–Si surface domains

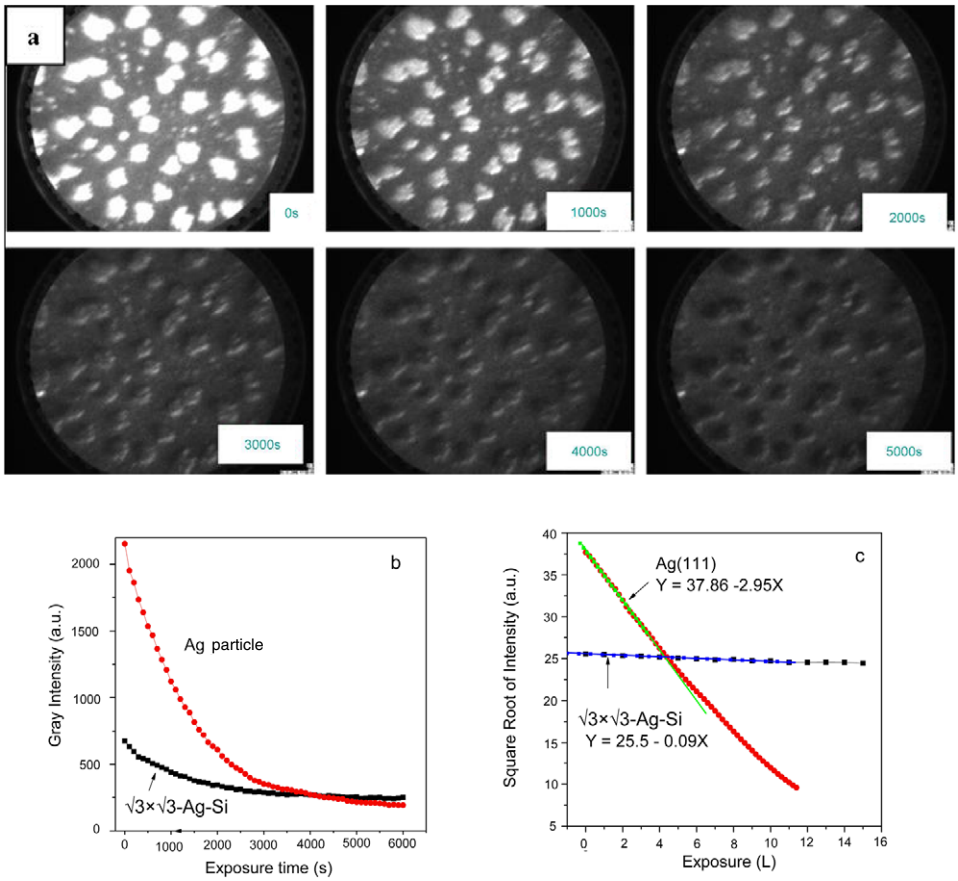

Figure 3. (a) Snapshots from the PEEM video acquired from the Ag | $\sqrt{3} \times \sqrt{3}$-Ag–Si surface exposed to different amounts of CCl_4 (FoV: 27 μm); (b) the variation of the gray intensity at the Ag particles and the bare $\sqrt{3} \times \sqrt{3}$-Ag–Si surface as a function of CCl_4 exposure time; (c) the evolution of the square root of the gray intensity of the PEEM images from the Ag(111) and $\sqrt{3} \times \sqrt{3}$-Ag–Si surfaces with CCl_4 exposure time.

remains almost constant except for a little decrease at the beginning of the CCl_4 dosing, which may be caused by CCl_4 reactions at small Ag particles scattered on the $\sqrt{3} \times \sqrt{3}$-Ag–Si surface. It has been shown that CCl_4 dissociation on Ag surfaces produces Cl species (figure 1), which will consequently increase the surface work function [19]. The significant change in the PEEM image contrast at the bulk Ag particles indicates a strong CCl_4 dissociation on the bulk Ag surface, while the unchanged PEEM image of the $\sqrt{3} \times \sqrt{3}$-Ag–Si surface suggests resistance of the surface to CCl_4 dissociative adsorption.

To illustrate more clearly the reaction dynamics on the bulk Ag and monolayer Ag surfaces, CCl_4 reactions on the well-defined bulk Ag(111) surface and the bare $\sqrt{3} \times \sqrt{3}$-Ag–Si surface at RT were investigated by PEEM under the same imaging conditions and the same CCl_4 exposure. The gray intensity data of the PEEM images from both surfaces were plotted as a function of CCl_4 exposure (figure 3(c)). Quantitative analysis of the data is given below.

The surface work function change ($\Delta\Phi$) presents a linear dependence on the coverage of the surface adsorbed Cl species (Θ) at low coverage approximation [9]. Furthermore, XPS results (not shown here) show that the amount of dissociated surface Cl is proportional to the CCl_4 exposure (E) in the case of low E. Accordingly, $\Delta\Phi$ will be linearly dependent on E, as described by the following equation:

$$\Delta\Phi = K \cdot E. \tag{1}$$

K is a parameter which is related to the rate constant of CCl_4 dissociative reaction on the Ag surfaces.

The image contrast observed in PEEM is directly related to the local variation of the surface photocurrent j. The photocurrent from a solid surface with a surface work function of Φ irradiated with photons, $h\nu$, can be described by the Fowler equation [20–22]:

$$j(h\nu) = q(h\nu - \Phi + F)^2 \tag{2}$$

q is the material dependent quantum efficiency and F is related to the electric field applied to the sample. Using equations (1) and (2) we get

$$j(h\nu) = q(h\nu - \Phi_0 - KE + F)^2. \tag{3}$$

Φ_0 is the initial surface work function before the surface reaction. The main UV line that we used is about 4.9 eV. For simplicity, we consider $h\nu$ as a constant. At the imaging condition, the electric field applied to the sample is also fixed. Thus, the following equation can be derived:

$$\sqrt{j(h\nu)} = m - nE. \tag{4}$$

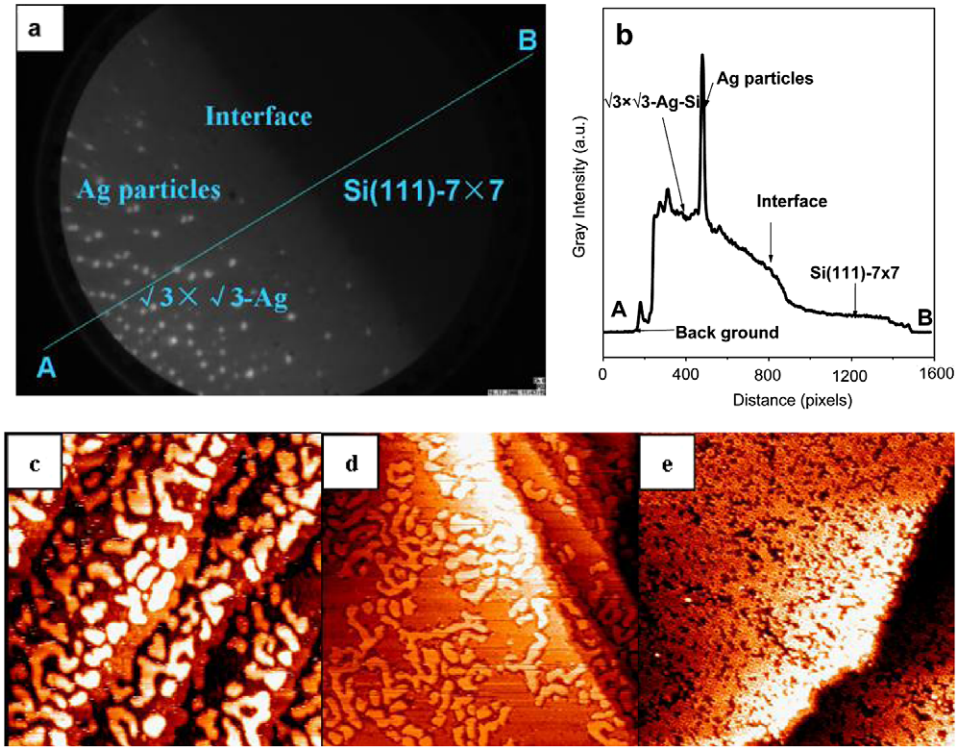

Figure 4. (a) PEEM image (FoV: 250 μm) of the Ag | $\sqrt{3} \times \sqrt{3}$-Ag–Si | Si(111)-7 × 7 surface, (b) gray intensity change along the line AB marked in (a), (c) STM image (200 nm × 200 nm) of the $\sqrt{3} \times \sqrt{3}$-Ag–Si surface region, (d) STM image (300 nm × 300 nm) of the interface region between $\sqrt{3} \times \sqrt{3}$-Ag–Si and Si(111), (e) STM image (100 nm × 100 nm) of the Si(111)-7 × 7 surface region.

Both m and n are constants, and n is a key parameter which characterizes the surface reactivity. Figure 3(c) shows the plots of the square root of the gray intensity, $\sqrt{j}$, as a function of CCl_4 exposure. The gray intensity of the bulk Ag surface decreased faster and it was finally lower than that of the monolayer Ag film surface. At low coverage, the two lines are linearly dependent on CCl_4 exposure, which is consistent with the relationship shown in equation (4). The linear fit of the data results in $n_{\text{bulk Ag}} = 2.95$ and $n_{\sqrt{3}\times\sqrt{3}\text{-Ag–Si}} = 0.09$. The quantitative analysis of the PEEM data definitely demonstrates that the reactivity of the bulk Ag surface to CCl_4 at RT is more than one order higher (32 times) than that on the $\sqrt{3} \times \sqrt{3}$-Ag–Si surface.

Another sample consisting of the $\sqrt{3} \times \sqrt{3}$-Ag–Si, bulk Ag, and Si(111)-7 × 7 surfaces was specially prepared by putting a shutter in front of the sample to mask half of the Si(111) surface during Ag deposition. On the sample surface, there are four surface regions: $\sqrt{3} \times \sqrt{3}$-Ag–Si, bulk Ag particles, Si(111)-7 × 7, and the transition region between the $\sqrt{3} \times \sqrt{3}$-Ag–Si and Si(111) (denoted as Ag | $\sqrt{3} \times \sqrt{3}$-Ag–Si | Si(111)-7 × 7). The four surface regions present different surface work functions, and have different PEEM image contrast as shown in figure 4(a). The gray intensity profile along the line labeled in the image was given in figure 4(b). Ag particles have the highest gray intensity due to the metallic nature, and the gray intensity of Si(111) is the lowest, just a little higher than the background because of its semiconductor nature and low DOS at E_F. The interface region consists of the Si(111) and $\sqrt{3} \times \sqrt{3}$-Ag–Si surface phases, and the brightness of this region is between the pure Si(111) and $\sqrt{3} \times \sqrt{3}$-Ag–Si surfaces. The assignment of the different surface regions is further attested to by STM. Figure 4(c) shows the STM image from the left region of the sample. The typical two-level surface structure indicates the $\sqrt{3} \times \sqrt{3}$-Ag–Si structure. Figure 4(e) displays the image from the right region of the sample, and the typical 7 × 7 surface atomic reconstruction can be seen. However, due to the contamination by the Ag deposition, many atomic defects were observed. Between the $\sqrt{3} \times \sqrt{3}$-Ag–Si surface and the Si(111)-7 × 7 surface is a transition region with a mixed surface structure of $\sqrt{3} \times \sqrt{3}$-Ag–Si and Si(111)-7 × 7, as shown in figure 4(d).

In situ PEEM was applied to study the reactivity of the Ag | $\sqrt{3} \times \sqrt{3}$-Ag–Si | Si(111)-7 × 7 surface to CCl_4. Figure 5(a) shows snapshots from the PEEM video acquired from the surface exposed to 5.2×10^{-9} mbar CCl_4 at RT. Like the result shown in figure 3, the image contrast between the Ag particles and $\sqrt{3} \times \sqrt{3}$-Ag–Si surfaces becomes inverted after CCl_4 exposure because of the sharp increase in the work function of Ag particles caused by dissociated atomic Cl [12, 19]. The decrease in the gray intensity of Si(111) is due to an increase in the surface work function and the extinction of the surface states by the dissociated Cl species [15]. The gray intensities of the surface regions labeled in figure 5(a) were plotted as a function of exposure time (figure 5(b)). Due to the low DOS near E_F the Si(111) surface presents quite low gray intensity in the PEEM image, contrasted with those at the Ag surfaces. For easy comparison, all the gray intensity curves

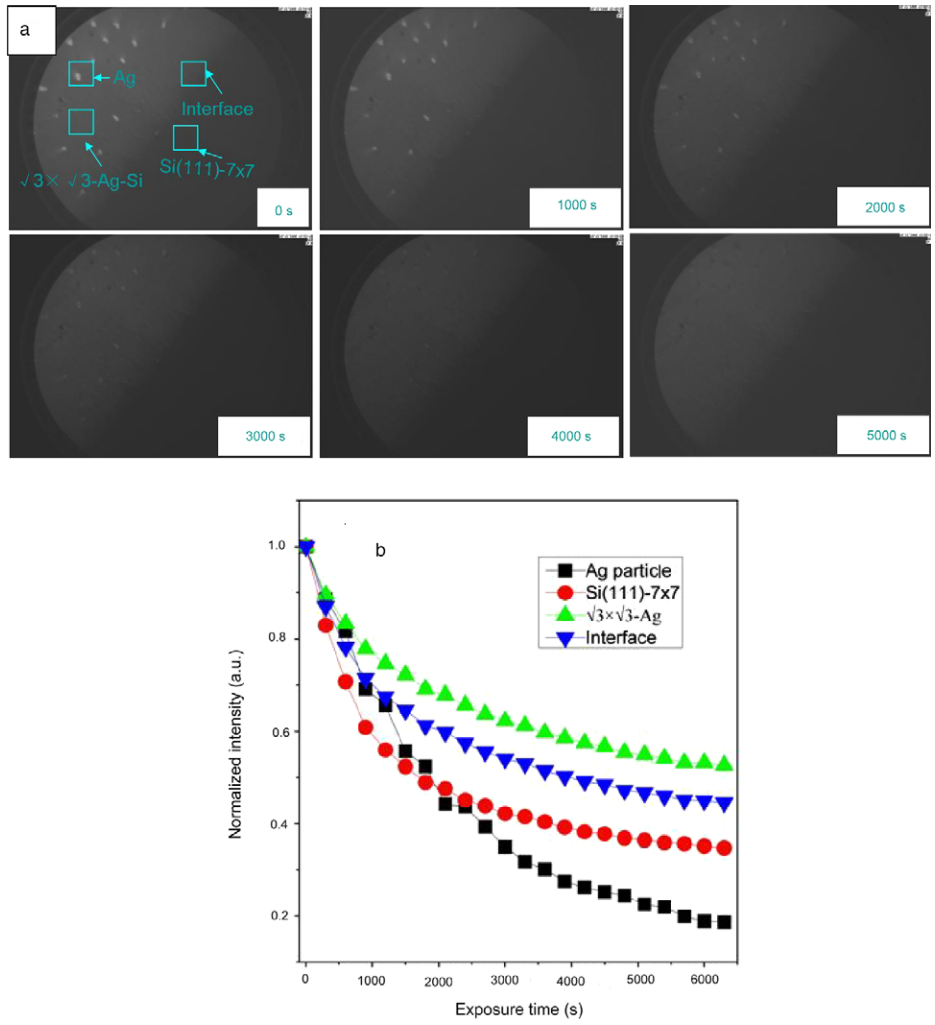

Figure 5. (a) PEEM images (FoV: 250 μm) of the Ag | $\sqrt{3} \times \sqrt{3}$-Ag–Si | Si(111)-7 × 7 surface exposed to different amounts of CCl_4. (b) Variation of the normalized gray intensity at the different areas labeled in (a) with exposure time.

have been normalized, and the rate of CCl_4 dissociation can be derived from the slope of the intensity curves at the initial stage of the CCl_4 exposure. The larger slope of the intensity curve from the Si(111) surface indicates the higher dissociation rate on this surface. The dynamic data in figure 5(b) lead to the conclusion that the surface reactivity order is Si(111) > bulk Ag ∼ AgSi interface > $\sqrt{3} \times \sqrt{3}$-Ag–Si, which agrees well with the TP-XPS and RT-XPS results (figure 1).

It has been revealed that CCl_4 adsorption on the Si(111)-7 × 7 follows the adatom–restatom pair adsorption mechanism. AT RT, the dangling bonds at the adatoms and restatoms favor the dissociation of CCl_4 into atomic Cl [15]. On the Ag(111) surface, CCl_4 adsorption happens with three chlorine atoms bonded to three surface Ag atoms and the fourth C–Cl bond aligned with the surface normal [19, 23]. With this adsorption configuration, the activation energy for the C–Cl bond dissociation is only 0.19 eV, and the dissociation is facilitated by the strong interaction among Cl valence electrons, Ag 4d electrons, and Ag 5sp electrons [12]. In particular, the charge transfer from the delocalized sp valence electrons to the approaching CCl_4 molecule is critical to the C–Cl bond breaking. At the $\sqrt{3} \times \sqrt{3}$-Ag–Si surface, the adsorbed Ag atoms render extinct all the dangling bonds of the Si(111)-7 × 7 surface. Moreover, the Ag 5sp electrons become confined at the $\sqrt{3} \times \sqrt{3}$-Ag–Si surface due to the presence of the Ag–Si interface, and could not transfer to gas adsorbates. Therefore, the lower reactivity at the $3 \times \sqrt{3}$-Ag–Si surface is very much expected as compared to those of the Ag(111) and Si(111) surfaces, because of the absence of Si dangling bonds and confinement of the free Ag 5sp electrons at the Ag monolayer film grown on Si(111).

4. Conclusions

CCl_4 dissociative reactions at the bulk Ag, Si(111), and $\sqrt{3} \times \sqrt{3}$-Ag–Si surfaces were studied by XPS and UV-PEEM. It has been found that strong dissociative adsorption of CCl_4 happens on the bulk Ag(111) and Si(111) surfaces but only molecular adsorption was observed on the $\sqrt{3} \times \sqrt{3}$-Ag–Si surface in the temperature range between 120 K and RT. The surface reactivity to CCl_4 follows the order of Si(111) > bulk

Ag > $\sqrt{3}\times\sqrt{3}$-Ag–Si. The low reactivity of the $\sqrt{3}\times\sqrt{3}$-Ag–Si surface can be attributed to the absence of Si dangling bonds and confinement of Ag 5sp electrons at the Ag–Si interface.

Acknowledgments

This work was financially supported by the National Natural Science Foundation of China (Nos 20603037, 20733008 and 20873143), Ministry of Science and Technology of China, and Chinese Academy of Sciences ('Bairen' program).

References

[1] Ertl G 2000 *Adv. Catal.* **45** 1
[2] Jakubith S, Rotermund H H, Engel W, Oertzen A and Ertl G 1990 *Phys. Rev. Lett.* **65** 3013
[3] Wolff J, Papathanasiou A G, Rotermund H H and Ertl G 2001 *Science* **294** 134
[4] Kim M, Bertram M, Pollmann M, Oertzen A, Mikhailov A S, Rotermund H H and Ertl G 2001 *Science* **292** 1357
[5] Imbihl R and Ertl G 1995 *Chem. Rev.* **95** 697
[6] Heringdort F J M, Reuter M C and Tromp R M 2001 *Nature* **412** 517
[7] Weidkamp K P, Tromp R M and Hamers R J 2007 *J. Phys. Chem.* C **111** 16489
[8] Huang W X, Zhai R S and Bao X H 2001 *Langmuir* **17** 3629
[9] Przychowski M D, Marx G K L, Frecher G H and Schönhense G 2004 *Surf. Sci.* **549** 37
[10] Hasegawa S, Tong X, Takeda S, Sato N and Nagao T 1999 *Prog. Surf. Sci.* **60** 89
[11] Chen L, Xiang H J, Li B, Zhao A, Xiao X, Yang J, Hou J G and Zhu Q 2004 *Phys. Rev.* B **70** 245431
[12] Yao Y X, Liu X, Fu Q, Li W X, Tan D L and Bao X H 2008 *ChemPhysChem* **9** 975
[13] Schmitsdorf R F and Mönch W 1996 *Surf. Sci.* **352** 322
[14] Saranin A A, Khramtsova E A and Lifshits V G 1993 *Surf. Sci. Lett.* **296** L21
[15] Yao Y X, Fu Q, Tan D L and Bao X H 2008 *Surf. Sci.* **602** 2183
[16] Junker K H, Hess G, Ekerdt J G and White J M 1998 *J. Vac. Sci. Technol.* A **16** 2995
[17] Piao H, Adib K and Barteau M A 2004 *Surf. Sci.* **557** 13
[18] Thürmer K, Williams E D and Reutt-Robey J E 2003 *Phys. Rev.* B **68** 155423
[19] Bovet N, Sayago D I, Allegretti F, Kröger E A, Knight M J, Barrett J, Woodruff D P and Jones R G 2006 *Surf. Sci.* **600** 241
[20] Fowler R H 1931 *Phys. Rev.* **38** 45
[21] Guth E and Mullin C J 1941 *Phys. Rev.* **59** 867
[22] Cai M, Langford S C, Wu M, Huang W, Xiong G, Droubay T C, Joly A G, Beck K M, Hess W P and Dickinson J T 2007 *Adv. Funct. Matter* **17** 161
[23] Zhang H, Fu Q, Yao Y X, Zhang Z, Ma T, Tan D L and Bao X H 2008 *Langmuir* **24** 10874